AIAA Paper 99-1714, Proceedings of the 15th CEAS/AIAA Aerodynamic Decelerator Systems Technology Conference and Seminar, Toulouse, France (1999).

3–D COMPUTATION OF PARACHUTE FLUID–STRUCTURE INTERACTIONS: PERFORMANCE AND CONTROL

Keith Stein[†], Richard Benney[‡]
U.S. Army Soldier and Biological Chemical Command,
Soldier Systems Center
Natick, Massachusetts 01760, USA

Tayfun Tezduyar[§]
Mechanical Engineering and Materials Science
Army HPC Research Center - Rice University
Houston, Texas 77005, USA

Vinay Kalro[¶]
Development Team – Fluent, Inc.
Evanston, Illinois 60201, USA

and

John Leonard[#], Michael Accorsi[**]
University of Connecticut
Storrs, Connecticut 06269, USA

ABSTRACT

We present a parallel computational strategy for carrying out 3–D simulations of parachute fluid–structure interaction (FSI), and demonstrate the strategy for simulations of airdrop performance and control phenomena in terminal descent. The strategy uses a stabilized space–time formulation of the time–dependent, 3–D Navier–Stokes equations of incompressible flows for the fluid dynamics (FD) solution. Turbulent features of the flow are accounted for using a zero–equation turbulence model. A finite element formulation derived from the principle of virtual work is used for the parachute structural dynamics (SD). Coupling of the FD with the SD is implemented over the the fluid–structure interface, which is the parachute canopy surface. Large deformations of the structure are handled in the FD mesh using an automatic mesh moving scheme.

[†] Aerospace Engineer

[‡] Aerospace Engineer, Senior Member

[§] James F. Barbour Professor in Engineering

[¶] Finite Element Specialist, Development Team

[#] Professor, Department of Civil & Environmental Engineering

[**] Professor, Department of Civil & Environmental Engineering, Member

INTRODUCTION

Fluid–structure interactions (FSI) are involved at all stages of airdrop systems performance, including at initial deployment, during inflation, at terminal descent (or gliding/maneuvering for steerable parachutes), and at soft landing (i.e., retraction for round parachutes, flared landing for ram–air parachutes). The interaction between the parachute system and the surrounding flow field is dominant in most parachute operations, and thus the ability to predict parachute FSI is necessary for accurate prediction of parachute behavior. This paper will describe current efforts to develop a general purpose computer model which can accurately predict 3–D FSI for various parachute systems under the different stages of performance. We will focus on the FSI performance during terminal descent stage to include control and maneuvering performance. Issues involved in performing simulations with the current model will be presented to include the finite element formulations, coupling strategies, mesh moving strategies, and implementation on parallel supercomputers.

We present a parallel computational strategy for carrying out 3–D simulations of parachute fluid–structure interaction (FSI), and demonstrate the strategy for simulations of airdrop performance and control phenomena in terminal descent. The strategy uses the Deforming–Spatial–Domain/Stabilized Space–Time (DSD/SST) formulation[1,2]

of the time–dependent, 3–D Navier–Stokes equations of incompressible flows for the fluid dynamics solution. Turbulent features of the flow are accounted for by using a zero–equation Smagorinsky turbulence model.[3] A finite element formulation derived from the principle of virtual work is used for the structural dynamics (SD).[4,5] The coupling of the FD with the SD is implemented over the fluid–structure interface, which is the canopy surface. Large deformations of the structure are handled in the FD mesh by using an automatic mesh moving scheme with remeshing as needed. The DSD/SST procedure is well suited for problems involving deforming domains (spatial domains changing with time), such as the deformations encountered during parachute FSI.[6] This formulation has been well tested and applied to a large variety of fluid dynamics problems involving moving boundaries and interfaces. In the space–time formulation, the finite element interpolation functions vary both spatially and temporally, automatically taking into account deformations in the spatial domain.

In recent years, the DSD/SST procedure has been applied to a variety of FSI problems. Preliminary DSD/SST simulations were successfully performed to simulate fluid–structure interaction behaviors for flow problems involving moving cylinders and aerofoils.[7,8] Later, the approach was applied to simulate the FSI response of a flexible pipe to internal flow[9] and to two–phase FSI flow problems including interior ballistics.[10] Recently, the approach has been used to predict the FSI response for the inflation of an axisymmetric cable–membrane parachute structure,[11] to predict the steady–state descent characteristics for a ram–air parachute system,[12] and to predict terminal descent characteristics for a T–10 parachute system.[13]

For the FSI problems presented, we will give special attention to the transfer of coupling information between "compatible" and "incompatible" FD and SD interface meshes (i.e., parachute canopy surface meshes). For "compatible" meshes, the FD and SD have nodally equivalent interface meshes and transfer of coupling is straightforward. For "incompatible" meshes, coupling information must be transfered through more sophisticated projection strategies.[14]

GOVERNING EQUATIONS

Fluid Dynamics

Let $\Omega_t \subset \mathbb{R}^{n_{sd}}$ be the spatial domain, where n_{sd} is the number of space dimensions, and let Γ_t denote the boundary of Ω_t. The subscript "t" implies the time–dependence of the spatial domain. The Navier–Stokes equations for incompressible flows are:

$$\rho\left(\frac{\partial \mathbf{u}}{\partial t} + \mathbf{u}\cdot\nabla\mathbf{u} + \mathbf{f}\right) - \nabla\cdot\boldsymbol{\sigma} = \mathbf{0} \quad \text{on } \Omega_t, \quad (1)$$

$$\nabla\cdot\mathbf{u} = 0 \quad \text{on } \Omega_t, \quad (2)$$

where ρ, $\mathbf{u}$, $\mathbf{f}$, and $\boldsymbol{\sigma}$ are the density, velocity vector, external body force, and stress tensor respectively. For the problems under consideration, the fluid is assumed Newtonian and the dynamic viscosity is modified locally using a Smagorinsky turbulence model. Dirichlet and Neumann–type boundary conditions are prescribed on $(\Gamma_t)_g$ and $(\Gamma_t)_h$ respectively, where $(\Gamma_t)_g$ and $(\Gamma_t)_h$ are complementary subsets of the boundary Γ_t. The initial condition on the velocity is divergence free.

Structural Dynamics

Let $\Omega_t^s \subset \mathbb{R}^{n_{sd}}$ be the spatial domain bounded by Γ_t^s. The boundary Γ_t^s is composed of $(\Gamma_t^s)_g$ and $(\Gamma_t^s)_h$. The equations of motion for the structural system are:

$$\rho^s\left(\frac{d^2\mathbf{y}}{dt^2} - \mathbf{f}\right) - \nabla\cdot\boldsymbol{\sigma}^s = \mathbf{0} \quad \text{on } \Omega_t^s, \quad (3)$$

where, $\mathbf{y}$, ρ^s, $\mathbf{f}$, and $\boldsymbol{\sigma}^s$ are the displacement vector, material density, external body forces, and Cauchy stress tensor, respectively. For the problems under consideration constitutive relationships are used assuming the materials are Hookean with linear–elastic properties, large displacements, and small strains.

FINITE ELEMENT FORMULATIONS

Fluid Dynamics

To handle the time–variant spatial domains encountered in parachute problems, we employ the DSD/SST finite element formulation. In this formulation, the finite element interpolation polynomials are functions of both space and time and the stabilized variational formulation of the problem is written over the associated space–time domain, automatically taking into account deformations in the spatial domain and protecting the computation against numerical oscillations. This method has been applied to a large number of problems with moving boundaries and interfaces. The interested reader is directed to Tezduyar et al.[1,2] for further details.

Structural Dynamics

A semi–discrete finite element formulation for the SD equations of motion is obtained from the principle of virtual work. Large geometric displace-

ments of the structure are handled by using a Lagrangian description of the problem. A variety of parachute–specific features have been incorporated into the SD solver in addition to membrane and cable elements to include concentrated mass elements (for payload representation), line and point drag force approximations, and time–variant cable lengths (for control line pulls, reefing, etc.). The interested reader is directed to Benney et al.[5,15] for further details.

Mesh–Moving Strategy

In order to handle changes in the spatial domain due to parachute canopy deformations, a suitable mesh–moving scheme is necessary. Efficient special purpose mesh–moving algorithms can be designed for problems where parachute motion is somewhat predictable. For example, Kalro and Tezduyar[12] utilized a algebraic scheme to handle the FSI–induced motions of a ram–air parachute system. A more general purpose mesh–moving scheme is needed for problems with arbitrary and complex deformations. We will use an automatic mesh–moving scheme for the problems presented. In this scheme, the fluid mesh is treated as a linearly–elastic "pseudo–solid" that deforms as dictated by the motion of the surface boundaries of the fluid domain.[16] This scheme introduces an additional computational cost associated with the mesh–moving equations, but is well suited for handling the complex geometries and arbitrary deformations in the parachute problems of interest.

FLUID–STRUCTURE COUPLING

The fluid–structure coupling occurs on the FSI interface, which is defined as the common boundary between the fluid and structure domains. For the problems presented, the FSI interface is the parachute canopy surface. Coupling is established by transferring velocity and displacements from the structure to the fluid, and returning the pressure contribution of the surface traction to the structure. Displacements from the SD solution are treated as Dirichlet boundary conditions in the pseudo–solid formulation for the mesh moving scheme. Surface velocities from the SD solution are treated as Dirichlet boundary conditions in the DSD/SST formulation for the fluid. In return, parachute nodal surface pressures are applied as external forces on the structure in the SD formulation. This transfer of coupling information is depicted in Figure 1. FSI information can be passed between the FD and SD solvers using "compatible" or "incompatible" meshes. Compatible meshes refer to the cases where the fluid–structure interface is represented by nodally equivalent surface meshes in the FD and SD models. Transfer of FSI information in this case is straight–forward due to the one–to–one mapping of the surface nodes. Incompatible meshes refer to cases where the interface is represented by different surface meshes in the FD and SD models. This approach has the benefit in that it allows for individual meshes to be made that are most suitable for each solver. However, incompatible meshes require a more sophisticated projection scheme for transfer of information across the fluid–structure interface. Incompatible approaches have been demonstrated by Farhat[14] and Kalro and Tezduyar.[12] These two approaches are depicted in Figure 2 for a parachute application with a fluid mesh (bottom) and compatible (upper left) and incompatible (upper right) SD meshes.

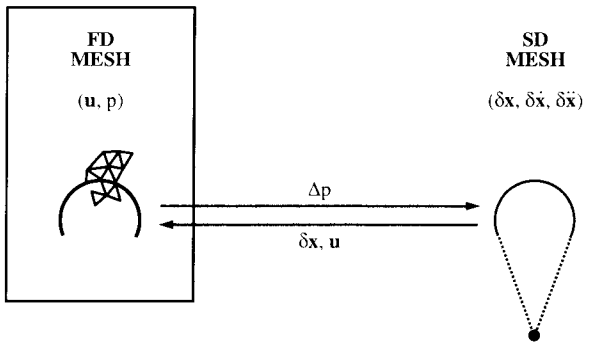

Figure 1. Tranfer of FSI information through interface mesh.

The general strategy for our coupling approach utilizes implicit solvers for both the SD and FD and is described below:

- Increment timestep
  - Form predictors for fluid and structure
  - FSI loop
    - Send pressures to structure
    - Newton–Raphson update for structure
    - Send velocity and displacement to fluid
    - Mesh motion
    - Newton–Raphson update for fluid
    - Repeat until converged
  - Form correctors for fluid and structure

IMPLEMENTATION

The FD and SD solvers are implemented using a message–passing paradigm and has been ported to a variety of architectures. Computations for the examples presented are carried out on the CRAY T3E-

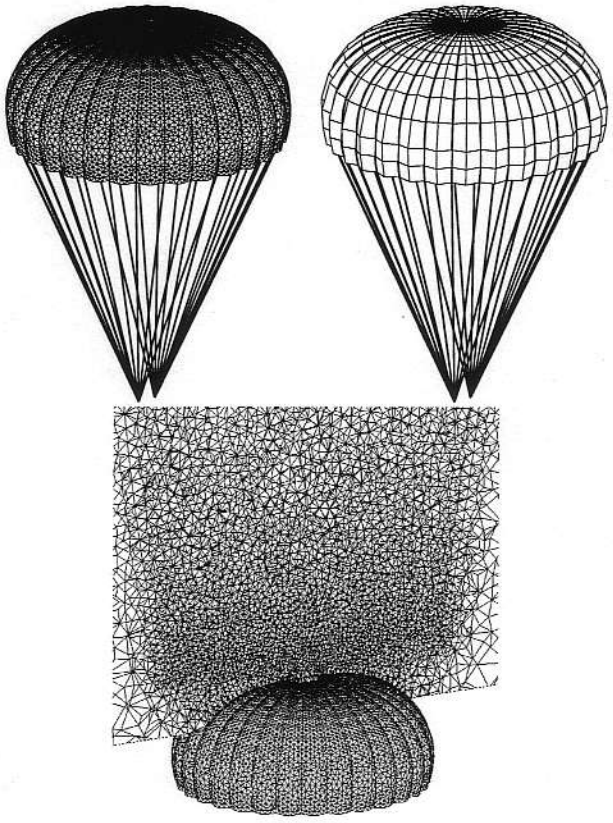

Figure 2. Parachute meshes: Compatible versus incompatible.

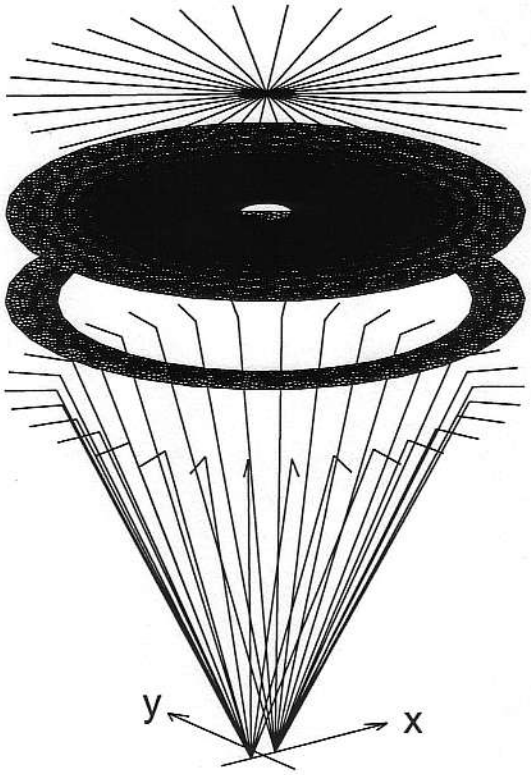

Figure 3. Compatible T–10 SD mesh.

1200 at the Army High Performance Computing Research Center (AHPCRC). The interested reader is directed to Kalro and Tezduyar[12] for further details.

NUMERICAL EXAMPLES: 3–D FSI FOR A T–10 PARACHUTE SYSTEM

The Army's T–10 personnel parachute system is a "flat extended skirt canopy" composed of a 35–foot diameter (D_c) canopy and 30 suspension lines each 29.4 feet long. The lines connect to two confluence points (which approximate the connection points for a personnel harness assembly). The suspension lines continue as 30 gore–to–gore reinforcements through the parachute canopy and meet at the apex. For the T–10, the extended skirt has a width which is $0.1D_c$ and a vent diameter of $0.1D_c$.

The following sections will demonstrate the 3–D FSI strategy for numerical examples involving the T–10 parachute system. First, we will compare numerical results for cases using compatible and incompatible meshes. Second, we will demonstrate the strategy for a T–10 parachute/payload system during terminal descent. Finally, we will demonstrate the ability to perform "line pulls" during a FSI simulation.

Compatible vs. Incompatible Meshes

SD Problem Setup:

A simulation was performed for two SD models for the T–10. The first SD model mesh (compatible case) consists of 9,183 nodes, 17,490 three–noded membrane elements for the unstructured canopy surface mesh, and 1,920 two–noded cable elements for the suspension lines and canopy reinforcements. This mesh results in 27,543 equations.

The second SD model mesh consists of 3,573 nodes, 780 nine–noded biquadratic membrane elements for the canopy surface mesh, and 1,170 two–noded cable elements for the suspension lines and canopy reinforcements. This mesh results in 10,713 equations. The parachute system is represented by linearly elastic materials, which have properties and dimensions representative of a T–10. Figures 3 and 4 show "blown–out" views for the compatible and incompatible SD meshes for the main canopy reinforcements (cables), the main canopy (membranes), the extended skirt (membranes), and the extended skirt reinforcements and suspension lines (cables).

A SD stand alone simulation was conducted for the unstructured mesh model to inflate the canopy

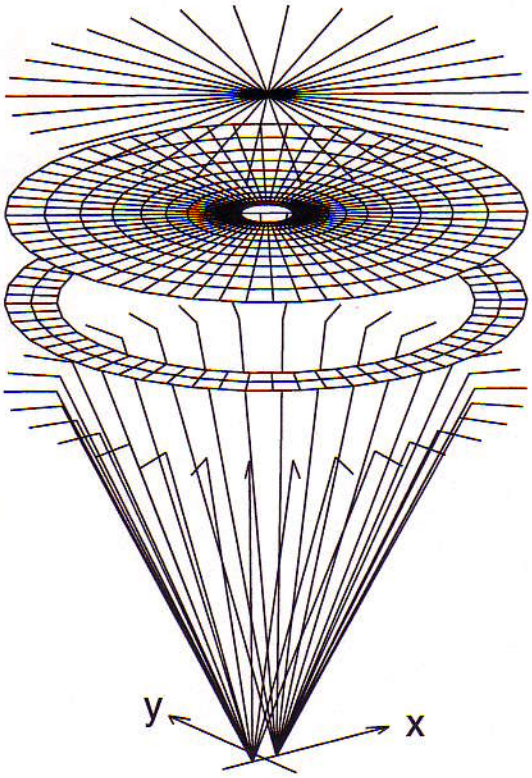

Figure 4. Incompatible T–10 SD mesh.

under a prescribed differential pressure of 0.5 lb/ft^2. Figure 5 shows the fully inflated static configuration for the T–10 model under the prescribed pressure loading. Maximum principal stresses for the parachute canopy (membrane) are superimposed on the surface, with low stresses along the canopy radial reinforcements and high stresses in the canopy midgore regions.

FD Problem Setup:

A 3–D tetrahedral volume mesh was generated using an unstructured finite element mesh generator[17] defining the three–noded membrane mesh for the T–10 canopy in its inflated configuration as an interior surface boundary. Canopy surface nodes were multiply defined, with one node for both the upper and lower surfaces. The mesh consists of 133,097 nodes and 783,910 tetrahedral elements, and results in 958,686 equations. Initial fully developed unsteady flow solutions were obtained for flow about the fixed canopy configuration at a Reynolds number of 5×10^6 (based on the constructed diameter of the T–10 canopy) using the DSD/SST procedure. Figure 6 shows the FD mesh and flowfield (velocity vectors and pressure field) in the $y = 0$ cutting plane and on the canopy surface. The developed flow solution was used as an initial condition for the FSI simulation.

Figure 5. Inflated T–10: SD geometry and stresses.

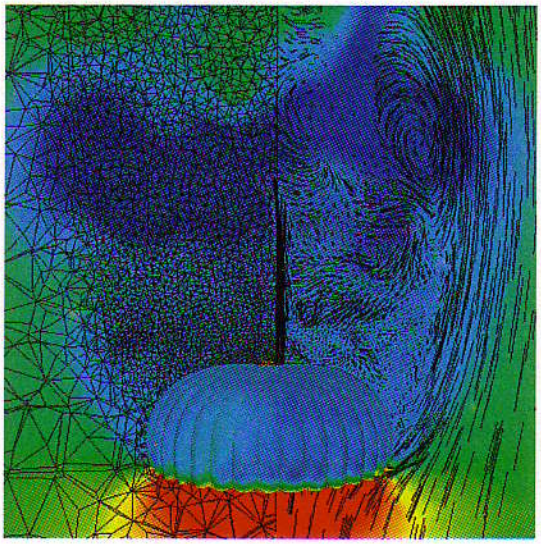

Figure 6. Inflated T–10: Initial FD mesh and flowfield.

FSI Simulation:

FSI simulations were conducted for both the "compatible" (unstructured triangular membrane mesh) and "incompatible" (biquadratic membrane mesh) SD models. The static solution for the compatible mesh from the standalone simulation was used as the initial geometry and initial velocities and accelerations were prescribed to be zero. In order to have the same starting conditions for the incompatible mesh, deflections were transferred from the compatible mesh static solution with the aid of a least–

squares projection. This projection occurs over the flat compatible and incompatible SD meshes which represent equivalent T–10 canopy surfaces. The fully developed flow field about the fixed configuration was used as the initial condition for the flow field. The two "payload" nodes in the SD model were fully constrained.

The coupled simulations were carried out with a nondimensional timestep size of 0.005, which equates to a dimensional timestep of 0.0032 seconds. The aerodynamic drag force acting on the canopy was calculated at each timestep. Figure 7 shows the time histories for the nondimensional drag force component. Good comparison is shown between the compatible and incompatible mesh simulations, with the incompatible mesh capturing higher–order modes of oscillation due to the higher–order biquadratic elements in the SD model. These oscillations are the result of the "snap through" of individual gores as the parachute settles during the initial stages of the FSI simulation. For the problem presented there is no membrane wrinkling model implemented and the triangular elements are unable to snap through for the given mesh resolution, whereas the higher order membranes can experience the snap through. Realistic wrinkling models are being developed[18] and we believe that these models will improve the correlation between compatible and incompatible meshes.

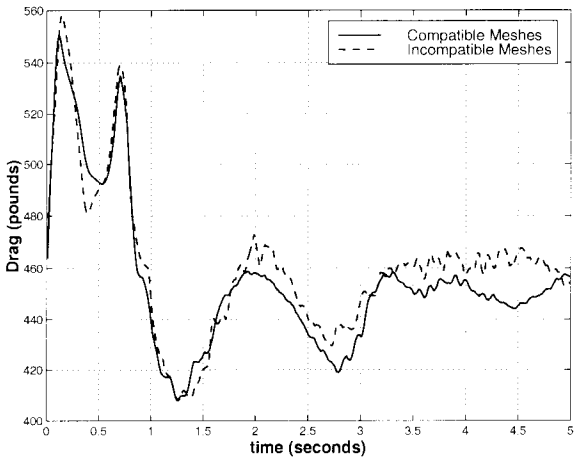

Figure 7. Drag histories for both the compatible and incompatible simulations.

Freefalling T–10 Parachute System

SD Problem Setup:

For this example, we modify the T–10 SD model to include a payload and a set of four risers connecting the payload to the suspension lines. We use the "incompatible" mesh from the previous example as

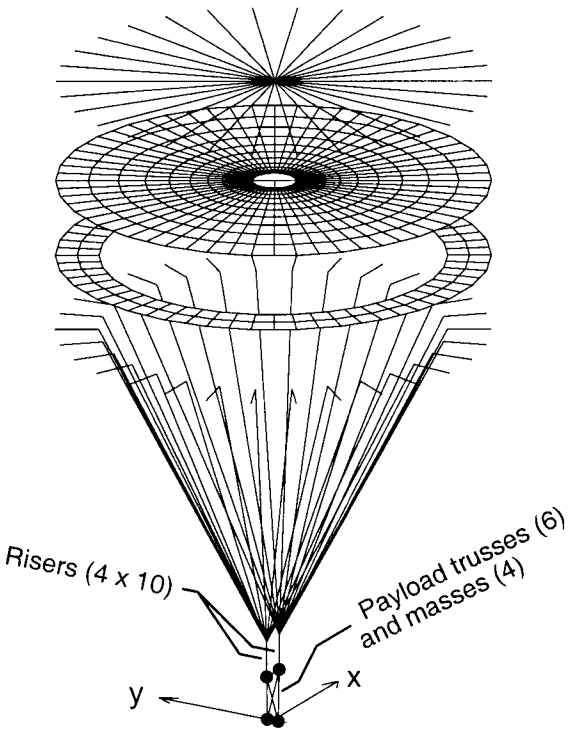

Figure 8. SD mesh for T–10 with risers and payload.

the base mesh for the parachute system. Each riser is represented by 10 additional two–noded cable elements. The front two risers each attach to seven suspension lines and the back risers each attach to eight suspension lines. Additionally, each front and back riser attaches to the payload. The payload is represented by a stiff tetrahedral truss system and four concentrated mass "elements." The six two–noded truss elements give the payload structure rigidity and the four concentrated masses approximate the mass of a typical paratrooper. This payload modeling technique has been used with good results for stand alone 3–D SD models.[15] The "blown out" depiction of the SD mesh for the T–10 parachute system with risers and payload is shown in Figure 8.

The SD model is broken into six distinct material groups; one membrane group, four cable groups, and a concentrated mass element group. The membrane group defines the parachute canopy. We have distinct cable groups for the suspension lines, the canopy radial reinforcements, the risers, and the payload trusses. The concentrated mass group is for the payload mass elements. The definitions for the different material groups are shown in Table 1.

A stand alone damped dynamic simulation was conducted for the T–10 parachute model to inflate the canopy under a prescribed differential pressure of 0.5 lb/ft^2. For the stand alone simulation, the four payload node points were fixed in space. The

	Cables		
Material Group	Suspension Lines	Radial Reinforcements	Risers
elements	780	360	40
thickness (area) ft (ft^2)	(0.0001)	(0.0001)	(0.0001)
density slugs/ft^3	6.0	6.0	6.0
Young's modulus lb/ft^2	4.32×10^6	4.32×10^6	2.16×10^7

	Cables	Membranes	Concentrated Masses
Material Group	Payload Trusses	Canopy	Payload Masses
elements	6	780	4
thickness (area) ft (ft^2)	(0.0001)	0.0001	—
density (mass) slugs/ft^3 (slugs)	2.0	6.0	(1.94)
Young's modulus lb/ft^2	4.65×10^9	2.0×10^5	—
Poisson ratio	—	0.3	—

Table 1. T–10 parachute system: Material properties.

equilibrium solution is used as the initial condition for the SD solver in the subsequent FSI simulation.

FD Problem Setup:

A 3–D tetrahedral volume mesh was generated, as in the previous example, using unstructured finite element mesh generation software. An unstructured triangular canopy surface mesh was generated by projecting displacements for the SD equilibrium solution onto a flat unstructured geometry for the T–10 canopy. This unstructured surface mesh is used to represent the T–10 canopy as an interior surface in the FD mesh. The mesh consists of 149,253 nodes and 888,344 tetrahedral elements and results in 1,087,826 equations. Initial fully developed unsteady flow solutions were obtained for flow about the fixed canopy configuration at a Reynolds number of 5×10^6 (which approximates terminal descent velocity of $22.0 ft/s$). The developed flow solution was used as an initial condition for the FSI simulation.

FSI Simulation:

For the previous example we simulated the FSI behavior for the flow about a T–10 parachute, where the "payload" was fixed in space. For this case, where the parachute is allowed to freefall, we define our boundary conditions as follows:

- Prescribed inflow velocity of $22.0 ft/s$
- Side boundaries have zero normal velocity and no shear stress
- Outflow velocity is stress–free
- Canopy surface has a no–slip condition (velocities obtained from SD solution)

It should be noted that for these conditions the parachute structure will fall (or rise) globally at a velocity relative to the inflow velocity. Thus, the predicted terminal descent for the parachute system will be the terminal SD velocity plus the inflow velocity. This combined Lagrangian–Eulerian description for the problem was selected to simplify the setup for the initial conditions of the FSI problem.

In order to handle the freefalling parachute, we handle our automatic mesh moving scheme as follows:

- Canopy surface mesh points have prescribed displacements equal to SD canopy displacements
- Outer mesh surfaces have prescribed displacements equal to the average SD canopy displacements (i.e., the FD mesh moves globally with the parachute canopy)
- Interior mesh points are moved based on the "pseudo–solid" automatic mesh moving scheme.

The FSI simulation is initiated using the equilibrium solution from the SD solver and the developed flow field from the FD solver. At the onset of the simulation, the payload nodes in the SD model are no longer fixed in space and the parachute SD model is fully nonconstrained. Motion of the structure is driven by the external forces (i.e., gravity, line drag, payload drag), the internal forces, and the FD–induced pressures on the canopy. Likewise, the FD solution is driven by the prescribed inflow condition and the SD–induced motions and velocities on the canopy surface boundary. The initial condition for the FSI simulation is not a coupled SD and FD equilibrium. Therefore, the parachute structure experiences a large amount of "settling" during the initial stages of the FSI simulation. Figures 9 and 10 show the behavior of the FD mesh and of the SD structure at four snapshots in time during the FSI simulation, with 0.63 seconds of real time between each snapshot. In Figure 9 we show the deforming canopy surface boundary in the FD mesh and the intersection of the FD mesh within a fixed cutting plane. The combined Lagrangian–Eulerian reference frame for the FSI simulation is evident by the fact that the canopy rises relative to the fixed cutting plane throughout the snapshop sequence. In Figure 10 we show the deforming T–10 structural model for the same four instants in time. We have attached an x–y coordinate system to $(x, y) = (0, 0)$ in the payload horizontal plane. Shown are the severe deformations in the parachute canopy and suspension lines. Also evident are motions of the payload system outside of the vertical axis. The figures also show the vertical position of the payload in feet for each snapshot.

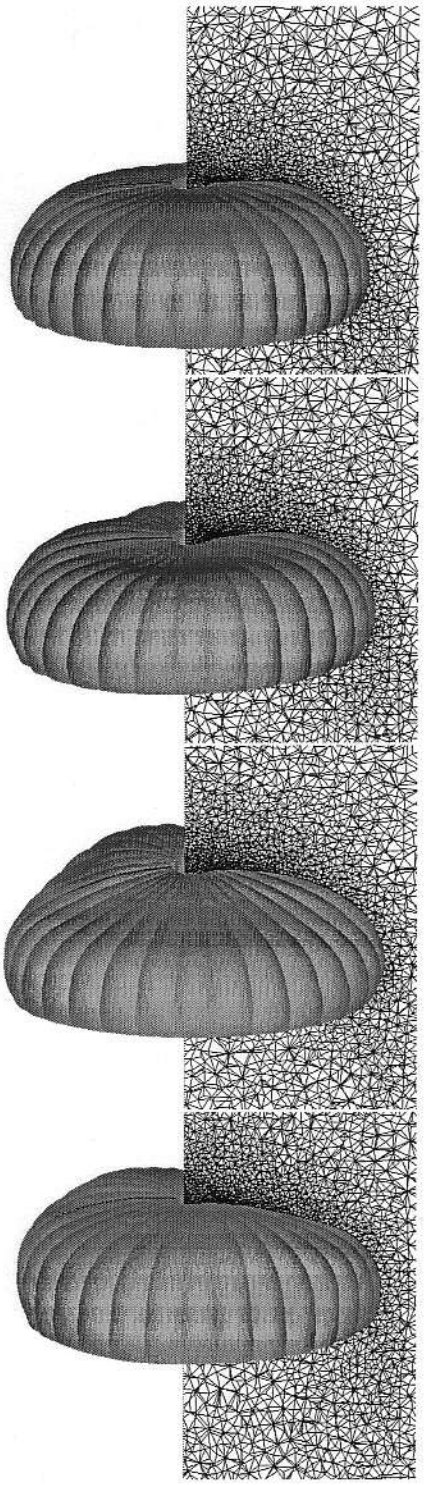

Figure 9. FD mesh during FSI simulation.

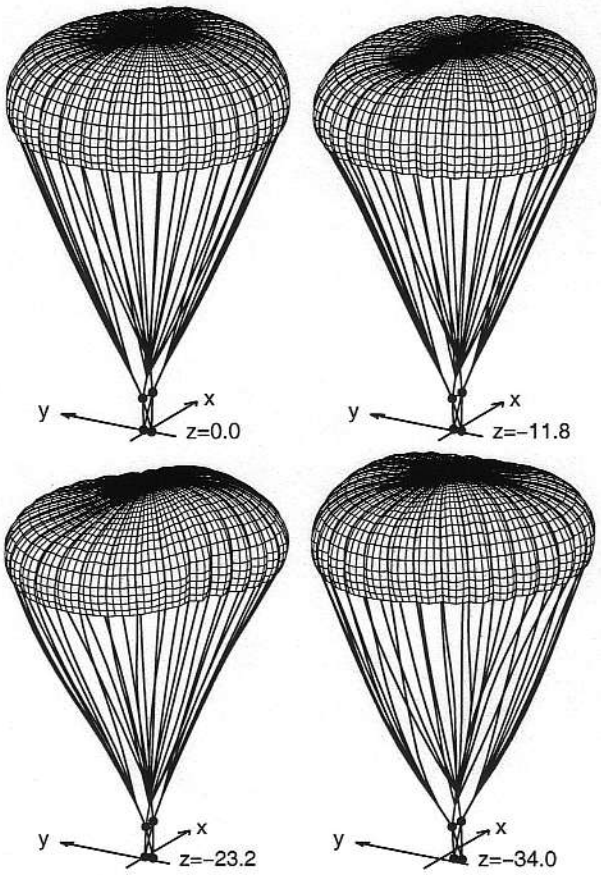

Figure 10. SD mesh during FSI simulation.

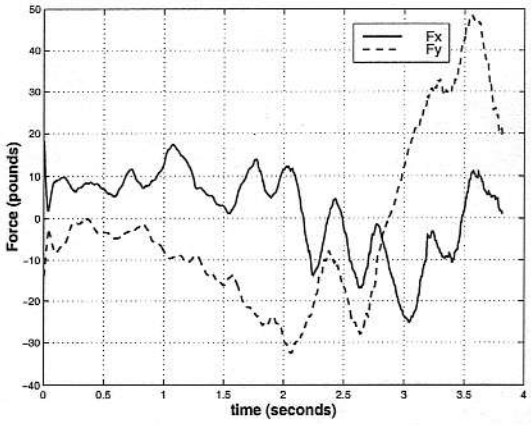

Figure 11. Horizontal components of aerodynamic force.

Figures 11 and 12 show the time histories of the pressure contribution to the aerodynamic force acting on the parachute canopy. Figure 11 shows the horizontal components of the aerodynamic force and indicates a nonaxial component of force which introduces oscillating and drifting behaviors in the parachute system. Figure 12 shows the vertical (or drag) component of the aerodynamic force and the total gravitational force acting on the parachute system (i.e., canopy, suspension lines, risers, and payload weights). As expected, the value for the drag force oscillates about the value of the weight for the

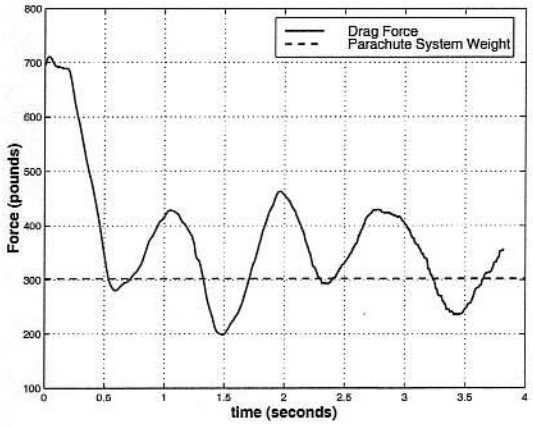

Figure 12. Vertical component of aerodynamic force.

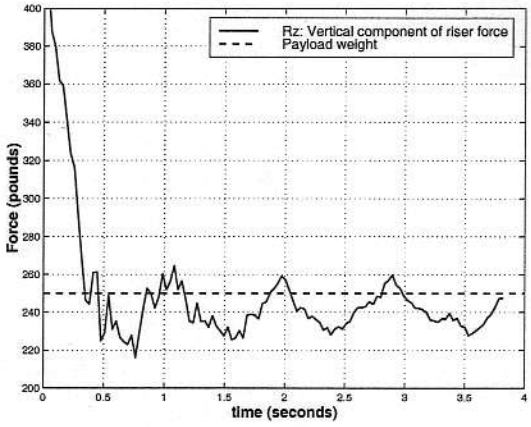

Figure 14. Net vertical component of riser forces.

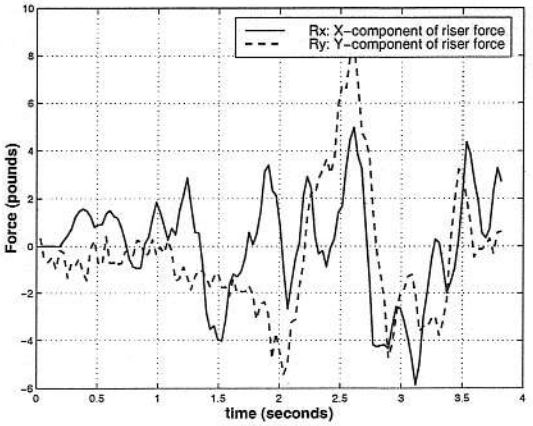

Figure 13. Net horizontal component of riser forces.

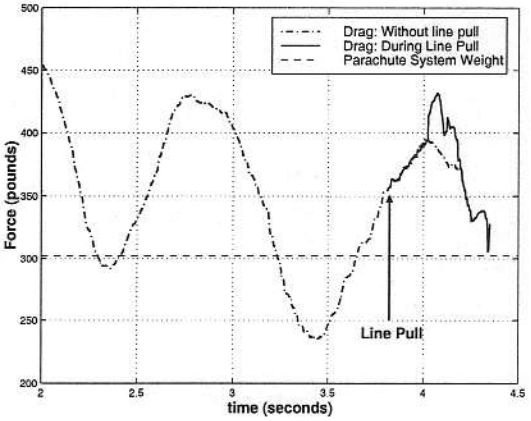

Figure 15. Soft landing drag force.

parachute system. Figures 13 and 14 show the time histories of the net tension forces that the risers exert on the payload. Figure 13 shows the net horizontal components of the riser forces and again indicates a nonaxial component of force acting on the parachute system. Figure 14 shows net vertical component of the riser forces. Since force contributions due to payload drag approximations are minimal, the net vertical component of the riser force effectively balances the 250–pound payload, which is evident in Figure 14.

T–10 Control Line Pull

The ability to represent time–variant cable lengths during an FSI simulation is necessary in order to represent several important parachute operations. These operations include control line "pulls" and "releases" in parachute maneuvering operations, riser pulls during softlanding, control line pulls for maneuvers and flared landings of ram–air parachutes, and dis–reefing operations. Numerical SD stand alone simulations for various control line operations have been reported by Benney et al.[15]

A "soft–landing" was simulated at the end of the T–10 FSI simulation presented in the previous section by smoothly decreasing the lengths of the four risers in time. During the simulation, the risers were each decreased from 3.0 feet to approximately 2.0 feet. Figure 15 shows the computed drag throughout the simulation with and without the line pull. As expected, higher drag is predicted for the line–pull case. This figure is a continuation of the drag history depicted in Figure 12.

Figure 16 shows the net vertical force in the four risers computed just before and throughout the soft landing simulation. This figure is a continuation of Figure 14.

Figure 17 shows the position of the payload throughout the entire freefall simulation, ending with the soft landing. The top portion of the figure shows the horizontal "drift" of the payload. The lower portion shows the vertical motion of the payload.

Figure 18 shows the velocity of the payload throughout the entire simulation. The top portion of the figure shows the horizontal velocity compo-

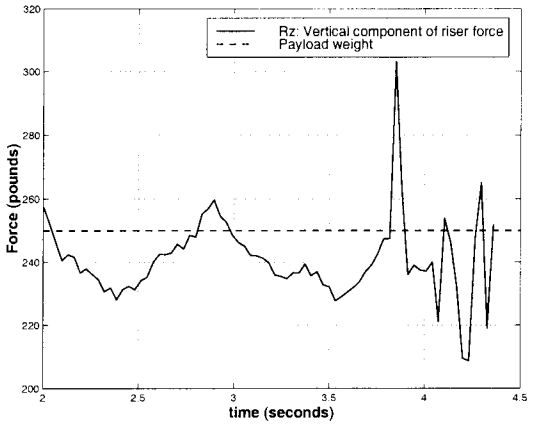

Figure 16. Soft landing net vertical riser force.

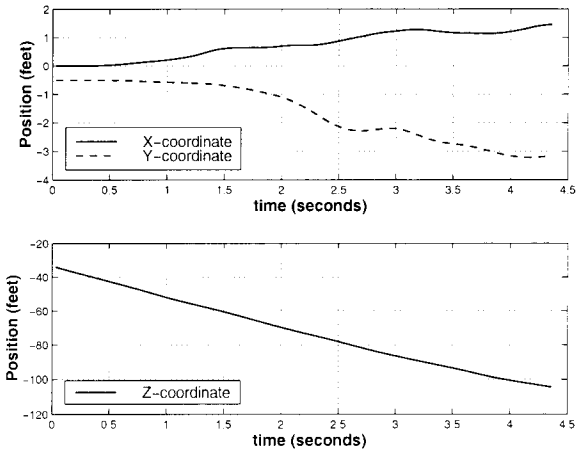

Figure 17. Soft landing payload position.

nents of the payload. The lower portion shows the vertical velocity of the payload. A deceleration due to the soft landing is evident.

CONCLUDING REMARKS

Parachute phenomena involve highly deformable structures interacting with complex flow fields. The ability to predict parachute phenomena requires the modeling of highly nonlinear FSI behaviors. This capability has only recently been attainable with advances in high performance computing methods and hardware. This paper has presented a methodology for carrying out simulations for parachute FSI that can be applied to a broad range of parachute applications. The FD model, SD model, and the coupling strategy undertaken have been described. Several test applications on a T–10 parachute were presented to demonstrate this capability. This work is continuing and further features will be added to include: improved mesh motion, mesh refinement,

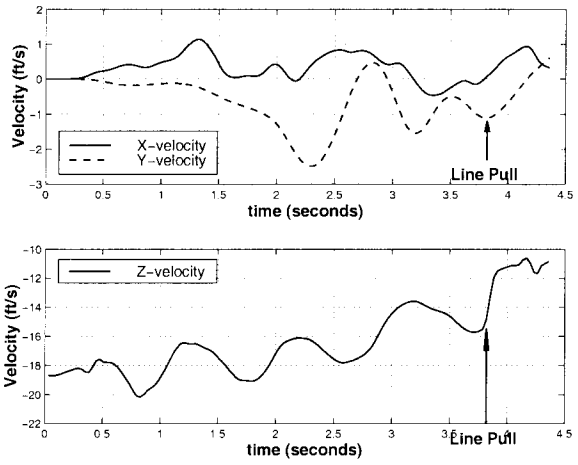

Figure 18. Soft landing payload velocity.

and remeshing of the FD domain; wrinkling algorithms,[18] improved material models, and contact algorithms for the SD model. Additionally, material porosity models will be incorporated in the future. Finally, a series of concurrent simulations,[19,20] wind tunnel experiments[20,21] and full–scale drop tests are being conducted to validate this parachute FSI simulation capability.

ACKNOWLEDGMENTS

This work was sponsored in part by NASA–JSC (grant number NAG9–1059), by AFOSR (contract number F49620–98–1–0214), and by the Army HPC Research Center under the auspices of the Department of the Army, ARL cooperative agreement number DAAH04–95–2–0003 and contract number DAAH04–95–C–0008. The content does not necessarily reflect the position or the policy of the Government, and no official endorsement should be inferred.

References

[1] T.E. Tezduyar, M. Behr and J. Liou, "A new strategy for finite element computations involving moving boundaries and interfaces – the deforming-spatial-domain/space-time procedure: I. The concept and the preliminary tests", *Computer Methods in Applied Mechanics and Engineering*, **94** (1992) 339–351.

[2] T.E. Tezduyar, M. Behr, S. Mittal and J. Liou, "A new strategy for finite element computations involving moving boundaries and interfaces – the deforming-spatial-domain/space-time procedure: II. Computation of free-surface flows, two-liquid flows, and flows with drifting cylinders", *Computer Methods in Applied Mechanics and Engineering*, **94** (1992) 353–371.

[3] J. Smagorinsky, "General Circulation Experiments with the Primitive Equations", *Monthly Weather Review*, **91** (1963) 99–165.

[4] R.J. Benney and J.W. Leonard, "A 3-D Finite Element Structural Parachute Model", *Proceedings of the 13th AIAA Aerodynamic Decelerator Systems Technology Conference*, Clearwater, 1995.

[5] R.J. Benney, K.R. Stein, J.W. Leonard and M.L. Accorsi, "Current 3-D Structural Dynamic Finite Element Modeling Capabilities", *Proceedings of the 14th AIAA Aerodynamic Decelerator Systems Technology Conference*, San Francisco, 1997.

[6] V. Kalro, S. Aliabadi, W. Garrard, T. Tezduyar, S. Mittal and K. Stein, "Parallel Finite Element Simulation of Large Ram–Air Parachutes", *International Journal for Numerical Methods in Fluids*, **24** (1997) 1353–1369.

[7] S. Mittal and T.E. Tezduyar, "A Finite Element Study of Incompressible Flows Past Oscillating Cylinders and Airfoils", *International Journal for Numerical Methods in Fluids*, **15** (1992) 1073–1118.

[8] S. Mittal and T.E. Tezduyar, "A Finite Element Study of Incompressible Flows Past Oscillating Cylinders and Airfoils", *Computer Methods in Applied Mechanics and Engineering*, **112** (1994) 253–282.

[9] S. Mittal and T.E. Tezduyar, "Parallel Finite Element Simulation of 3D Incompressible Flows – Fluid-Structure Interactions", *International Journal for Numerical Methods in Fluids*, **21** (1995) 933–953.

[10] G. Wren and S. Ray and S. Aliabadi and T. Tezduyar, "Simulation of Flow Problems with Moving Mechanical Components, Fluid-Structure Interactions and Two-Fluid Interfaces", *International Journal for Numerical Methods in Fluids*, **24** (1997) 1433–1448.

[11] K.R. Stein, R.J. Benney, V. Kalro, A.A. Johnson and T.E. Tezduyar, "Parallel Computation of Parachute Fluid–Structure Interactions", *Proceedings of the 14th AIAA Aerodynamic Decelerator Systems Technology Conference*, San Francisco, 1997.

[12] V. Kalro and T. Tezduyar, "A Parallel Finite Element Methodology for 3D Computation of Fluid–Structure Interactions in Airdrop Systems", *Proceedings of the 4th Japan-US Symposium on Finite Element Methods in Large-Scale Computational Fluid Dynamics*, Funabashi, Japan, 1998.

[13] K. Stein, R. Benney, V. Kalro, T. Tezduyar, J. Leonard, and M. Accorsi, "Parachute Fluid–Structure Interactions: 3–D Computation", ~~to appear in~~ *Computer Methods in Applied Mechanics and Engineering.* **190** (2000) 373-386.

[14] N. Maman and C. Farhat, "Matching Fluid and Structure Meshes for Aeroelastic Computations: A Parallel Approach", *Computers and Structures*, **54** (1995) 779–785.

[15] R. Benney, K. Stein, W. Zhang, M. Accorsi, J. Leonard, "Controllable Airdrop Simulations Utilizing a 3–D Structural Dynamics Model", *Proceedings of the CEAS/AIAA 15th Aerodynamic Decelerator Systems Technology Conference*, AIAA-99-1727, Toulouse, France, 1999.

[16] T.E. Tezduyar, M. Behr, S. Mittal, and A.A. Johnson, "Computation of Unsteady Incompressible Flows with the Stabilized Finite Element Methods–Space-Time Formulations, Iterative Strategies and Massively Parallel Implementations", *New Methods in Transient Analysis*, (eds. P. Smolinski, W.K. Liu, G. Hulbert and K. Tamma), AMD–Vol. 143, ASME, New York (1992) 7-24.

[17] A.A. Johnson and T.E. Tezduyar, "Parallel Computation of Incompressible Flows with Complex Geometries", *International Journal for Numerical Methods in Fluids*, **24** (1997) 1321–1340.

[18] M. Accorsi, K. Lu, J. Leonard, R. Benney, and K. Stein, "Issues in Parachute Structural Modeling: Damping and Wrinkling", *Proceedings of the CEAS/AIAA 15th Aerodynamic Decelerator Systems Technology Conference*, AIAA-99-1729, Toulouse, France, 1999.

[19] J. Sahu, H. Edge, K. Heavey, S. Chakravarthy, K. Stein, and R. Benney, "Comparison of Numerical Flow Field Predictions for Army Airdrop Applications", *Proceedings of the CEAS/AIAA 15th Aerodynamic Decelerator Systems Technology Conference*, AIAA-99-1715, Toulouse, France, 1999.

[20] K. Stein, R. Benney, V. Kalro, T. Tezduyar, T. Bretl, and J. Potvin, "Fluid–Structure Interaction Simulations of a Cross Parachute: Comparisons of Numerical Predictions with Wind Tunnel Data", *Proceedings of the CEAS/AIAA 15th Aerodynamic Decelerator Systems Technology Conference*, AIAA-99-1725, Toulouse, France, 1999.

[21] B. Brocato, L. Esteve, D. Garcia, C. Manglano, G. Peek and J. Potvin, R. Benney and K. Stein, R. Alamat and J. Little, "Experimental Study of Fluid–Structure Interactions on a Cross Parachute: Comparison of Wind Tunnel Data and Drop Data with CFD Predictions", *Proceedings of the CEAS/AIAA 15th Aerodynamic Decelerator Systems Technology Conference*, AIAA-99-1737, Toulouse, France, 1999.